Clays and Clay Minerals, Vol. 55, No. 1, 71–88, 2007.

KINETICS OF CITRATE-INDUCED SELENITE DESORPTION FROM MONTMORILLONITE AS AFFECTED BY COMPLEXATION WITH HYDROXYALUMINUM AND HYDROXYALUMINOSILICATE IONS

UTTAM KUMAR SAHA, L. M. KOZAK AND P. M. HUANG*

Department of Soil Science, University of Saskatchewan, 51 Campus Drive, Saskatoon, SK, S7N 5A8, Canada

Abstract—The citrate-induced desorption kinetics of pre-adsorbed Se from montmorillonite (Mt) and its complexes with hydroxyaluminum (HyA-Mt) and hydroxyaluminosilicate (HAS-Mt) were studied. The mole fraction of pre-adsorbed Se released in 24 h from different clays followed the trends of Mt >> HAS-Mt > HyA-Mt with a significant increase with elevated citrate concentration in the desorbing solution. In contrast, the amount of Se adsorbed per unit mass of different clays followed a clear-cut opposite trend of HyA-Mt > HAS-Mt >> Mt. The Se desorption kinetics in different systems indicated multiple rate characteristics; where an initial fast reaction (0.25−2 h) was followed by a slow reaction (2−16 h). Of the six different kinetic models tested (zero-, first-, and second-order; power function, Elovich, and parabolic diffusion), the second-order rate equation showed the overall best fit to the fast and slow desorption kinetic data from the clays. Based on second-order rate constants, the rates of the mole fraction of Se desorption by citrate from different clay systems at 298 K followed the order Mt > HAS-Mt >> HyA-Mt. For both fast and slow reaction, the rates of desorption increased proportionally with the level of citrate. Replicate experiments conducted across a range of temperature (288−318 K) yielded Arrhenius parameters that followed the order HyA-Mt > HAS-Mt >> Mt. Considering that a lower mole fraction of Se desorption after a particular reaction period, slower desorption kinetics, and a greater activation energy of desorption are the indices of increased adsorption bond strength, the results clearly indicate that HyA- and HAS-interlayering and coatings on Mt not only augmented its Se adsorption affinity and capacity, but also increased the adsorption bond strength. Silication in HyA not only reduced the Se adsorption capacity, but also weakened the adsorption bond strength. This establishes a significant role of HyA/HAS-interlayering and coating on Mt in influencing the rate of citrate-induced release of Se. Reduction in surface-positive potential following citrate adsorption on the clay surface, a direct ligand exchange between Se and citrate, and structural dissolution are possible mechanisms responsible for citrate-induced Se desorption in the present study.

Key Words—Citrate, Desorption, Hydroxyaluminosilicate, Hydroxyaluminum, Kinetics, Montmorillonite, Selenite.

INTRODUCTION

Selenium is both a toxic and essential element for animals and humans. A rigorous understanding of the environmental chemistry of Se is a special concern of the present day because of its dual importance to our life and the emerging reports of its deficiency and toxicity in nature.

Animals and humans predominantly acquire Se through the ingestion of plant materials. Based on the redox conditions, the two oxyanionic forms of Se such as selenite (SeO_3^{2-}) and selenate (SeO_4^{2-}) are plant bioavailable in soils. Under alkaline and well-oxidized conditions, selenate predominates, whereas selenite is favored under mildly oxidized and acidic conditions (Dynes and Huang, 1995). Furthermore, these two oxyanions may have different degrees of protonation depending on ambient pH. While selenate (pK_2 = 1.7, Lide, 2004) exists predominantly in an unprotonated state (SeO_4^{2-}) in most soil solutions, selenite occurs at different degrees of protonation depending on solution pH according to the following equilibria:

$$pK_1 = 2.62 \text{ (Lide, 2004)}$$
$$H_2SeO_3 \rightleftharpoons HSeO^-_3 + H^+$$
$$pK_2 = 8.32 \text{ (Lide, 2004)}$$
$$HSeO_3^- \rightleftharpoons SeO_3^{2-} + H^+$$

Selenate is weakly retained by soil colloidal particles and hence readily available for plant uptake. In contrast, selenite is strongly adsorbed onto the soil colloidal surfaces and hence represents a persistent source of bioavailable Se. Understanding and predicting Se bioavailability require knowledge and information on the processes controlling its transformation and transport in soils and associated environments. Sorption-desorption reactions at the soil particle-water interface exert a dominant influence on the solution concentration of metals, metalloids and other inorganics in soil and associated environments (Sparks, 2003). Like other metals and metalloids, a great deal of literature is

* E-mail address of corresponding author:
huangp@sask.usask.ca
DOI: 10.1346/CCMN.2007.0550106

available on the adsorption behavior of Se onto various natural and synthetic adsorbents (Hayes *et. al.*, 1987; Neal *et al.*, 1987a; Neal and Sposito, 1989; Saeki and Matsumoto, 1994; Dynes and Huang, 1997). The influences of organic and inorganic ligands on the adsorption of Se by soils and soil colloids have also been reported (Neal *et al.*, 1987b; Dynes and Huang, 1995, 1997). However, the influence of ionic environments on the desorption kinetics of Se from soils and soil colloids is only poorly known, even after repeated emphasis on its essentiality to a better understanding of the mobility, transport and fate of metals and metalloids in the natural environments. Indeed, this is, in general, true for all the metals, metalloids, and other inorganics of environmental concern. As noted by Scheidegger and Sparks (1996), more research is needed on desorption phenomena.

Understanding the release of a metal or metalloid from the solid phases of soils into soil solutions and their subsequent uptake by plants requires knowledge of the processes by which the metal or metalloid reaches the rhizosphere (Cushman, 1982). Rhizospheric reactions are known to play an important role in micronutrient acquisition (Curl and Truelove, 1986). The release of organic acids and other root exudates may influence solubility and uptake of the ions of nutrients and pollutants indirectly through their effects on microbial activity, rhizosphere physical properties and root growth patterns, and directly by acidification, complexation and chelation, ligand-exchange, precipitation-dissolution, and oxidation-reduction reactions (Uren and Reisenauer, 1988). A wide variety of low-molecular-weight organic acids (LMWOAs) have been identified in the soil rhizosphere, including oxalic, citric, acetic, malic, succinic, fumaric, *etc.* (Szmigielska *et al.*, 1995, 1997). The specific organic acids present and their concentrations determine the degree to which soil processes are affected. It has been reported that concentrations of LMWOAs in soil solution are in the range of 4×10^{-4} to 1×10^{-3} M (Stevenson, 1994). However, concentrations of LMWOAs much greater than millimolar would be expected to be produced in localized zones where biological activity is intense such as in the immediate vicinity of the root-soil interface, *i.e.* rhizosphere (Rovira, 1969; Stevenson, 1991) and near decomposing plant residues (Bruckert and Jacquin, 1969). The LMWOAs such as citric and oxalic, which form stable complexes with metals, will have a greater impact on the metal solubilization than those that do not form stable complexes (Krishnamurti *et al.*, 1997). These acids would also be more efficient in mobilizing the surface-complexed anions by ligand-exchange mechanisms. Organic acids are ubiquitous at the soil-root interface in all agricultural soils and related ecosystems. However, little is known of their impacts on the dynamics and mechanisms of Se release.

In this study, the citrate-induced desorption kinetics of pre-adsorbed Se from montmorillonite (Mt), hydroxy-aluminum (HyA; OH/Al = 2.0 and Si/Al = 0.00)-Mt and hydroxyaluminosilicate (HAS; OH/Al = 2.0 and Si/Al = 0.48)-Mt were investigated. These clays have been chosen, since HyA and HAS interlayers/coatings on montmorillonites (Mt) and vermiculites (Vt) are very common in acid to slightly acid soils (Lou and Huang, 1988, 1994, 1995; Matsue and Wada, 1988; Bautista-Tulin and Inoue, 1997) and such interlayering/coating causes a drastic modification of the charge and surface characteristics, ion adsorption, and ion-exchange behavior of the host clays (Harsh and Doner, 1984; Barnhisel and Bertsch, 1989; Inoue and Satoh, 1992, 1993; Sakurai and Huang, 1998; Lothenbach *et al.*, 1997; Saha and Inoue 1997; Saha *et al.*, 1998, 2002). Different concentrations of citrate were chosen as the desorbing agent, since citrate is one of the major organic ligands in the rhizosphere (Stevenson, 1967; Szmigielska *et al.*, 1997). This study addresses the consequences of dual factors on the desorption phenomena: (1) the relationship of citrate concentration with the rates of desorption of pre-adsorbed Se from the clays; and (2) the influence of complexation of Mt with HyA and HAS polymers and associated alteration of charge and surface properties on the rate, heat of activation, and pre-exponential factor of citrate-induced desorption of Se.

MATERIALS AND METHODS

Preparation of the adsorbents

The methods of preparation for the HyA/HAS-Mt complexes have been described in detail previously (Saha *et al.*, 2004). However, a brief description is given below. The colloidal fractions (<2 μm) of Mt clays collected from Hojun bentonite (Gunma, Japan) by repeated dispersion, sedimentation, and siphoning were successively (1) treated with dithionite-citrate (Mehra and Jackson, 1960) and 2% Na_2CO_3 (Jackson, 1979) to remove Fe oxides; (2) washed four times in 1 M CH_3COONa-1 M NaCl (pH 5) to Na saturate the exchange complex; (3) rinsed with 80% methanol until free of Cl^-; and (4) rinsed with acetone. The Na-saturated Mt clays were then air dried and gently ground in an agate mortar.

For HyA ionic solution, 0.1 M $AlCl_3$ solution was titrated with 0.1 M NaOH at the rate of 0.2 to 0.5 mL min^{-1} with continuous stirring to give a NaOH/Al molar ratio of 2.0. For HAS ionic solution, orthosilicic acid prepared from tetraethyl orthosilicate (Farmer *et al.*, 1979) was mixed with a 0.1 M $AlCl_3$ solution to obtain a Si/Al molar ratio of 1.00. The solution was then titrated with 0.1 M NaOH in the manner described above to give the same NaOH/Al molar ratio of 2.0. Both the HyA and HAS solutions were diluted to 2 L (final Al concentration $\approx$ 4 mM) and aged for 7 days at 293 K. The pHs of the solutions were recorded and clear filtrates were obtained by passing through a 0.2 μm pore size cellulose-NO_3 membrane filter (Toyo-Roshi Co.,

Tokyo) to remove the solid particles of $Al(OH)_3$ or any aluminosilicates. The Al and Si concentrations in the filtrates were determined (Lou and Huang 1994). The OH/Al and Si/Al molar ratios, pH, and Al concentrations of the HyA and HAS parent solutions reacted with Mt are presented in Table 1.

The HyA/HAS-Mt complexes were obtained through repeated reaction between Na-saturated Mt and the HyA or HAS solution as described by Inoue and Satoh (1993). The complexes were then made Cl^--free through washing with 80% methanol, washed with acetone, air dried, gently ground, and passed through a 0.246 mm sieve. The amounts of Al and Si fixed on the Mt were estimated as the difference between that present in the solution initially and that remaining in the solution after reacting with the clay.

Characterization of the adsorbents

The negative charge characteristics of Mt and HyA/HAS-Mt complexes were determined by measurement of Ca^{2+} retained in the pH range of 4−7.5 following the procedure described by Wada and Okamura (1980), with $CaCl_2$ substituted for NH_4Cl as the saturating solution (see also Inoue and Satoh, 1993). The PZSE of the HyA/HAS-Mt complexes was determined by a modified salt-titration method (Sakurai *et al.*, 1988). The total and external surface areas of the clay samples were determined by the ethylene glycol mono-ethyl ether (EGME) method (Eltantawy and Arnold, 1973) and by adsorption of N_2 gas at 78 K using a BET surface area analyzer (Shibata P-850, Shibata-Kagaku Co., Tokyo), respectively. The internal surface area was calculated as the difference between total and external surface areas.

X-ray diffraction (XRD) analysis of the parallel oriented clay specimens was performed under K- and Mg-saturated conditions with a Rigaku X-ray diffractometer RAD-1A (Rigaku Co., Tokyo) using Fe-filtered CoKα radiation generated at 30 kV and 10 mA. The XRD patterns were also recorded on the K-saturated specimens after heating at 383, 573 and 823 K and on the Mg-saturated specimens after solvation with glycerol.

The clay specimens were also examined by IR absorption spectroscopy. One milligram of air-dried sample was mixed with 200 mg of oven-dried and desiccated KBr and the KBr pellets were then examined by a Fourier-transform infrared (FTIR) spectrometer (Bio-Rad, Cambridge, MA).

Kinetics of Se desorption

Attainment of an equilibrium adsorption of Se on Mt, HyA-Mt and HAS-Mt always preceded the study of its desorption kinetics from the clays. The kinetics of Se desorption induced by different levels of citric acid (0, 5×10^{-6}, 5×10^{-5} and 5×10^{-4} M) in 0.01 M $NaNO_3$ were studied at pH 4.5 at 298 K. The effect of temperature on the kinetics of Se desorption from the

Table 1. Characteristics of the parent hydroxyaluminum (HyA) and hydroxyaluminosilicate (HAS) ionic solutions and the resultant HyA-montmorillonite (Mt) and HAS-Mt complexes.

Sample	Characteristics of the parent soutions					Characteristics of the HyA or HAS adsorbed on Mt			CEC		PZSE[a]	Surface area		
	OH/Al molar ratio	pH	Concentration of Si	Concentration of Al	Si/Al molar ratio	Amount of Si adsorbed	Amount of Al adsorbed	Average positive charge per Al atom	OH/Al molar ratio	Si/Al molar ratio	pH 4.0	pH 7.5		Internal	External	Total
			mM			mol kg^{-1} Mt					$cmol_c$ kg^{-1}			m^2 g^{-1}		
Mt	–	–	–	–	–	–	–	–	–	–	59.7	65.4	n.d.	529	72	601
HyA-Mt	2.0	4.15	0.00	3.96	0.00	0.00	1.13	0.36	2.64	0.00	18.9	52.6	4.7	322	128	450
HAS-Mt	2.0	4.48	3.80	3.82	0.99	0.66	1.37	0.21	2.79	0.48	31.1	43.9	4.4	379	108	487

[a] Point of zero salt effect
n.d. not determined

clays was also studied using a particular level (5×10^{-6} M citric acid in 10^{-2} M $NaNO_3$, pH 4.5) of citrate as the desorbing solution.

The Se adsorption kinetics onto these clays revealed that an equilibrium in Se adsorption was invariably reached after a 24 h reaction period (data not shown). Both adsorption and desorption were studied by a conventional batch method. All the experiments were carried out in duplicate. Details of the experimental procedure are given below.

An equilibrium Se adsorption on Mt and HyA/HAS-Mt complexes was achieved by reacting the clays with a selenite-containing bathing solution for a 24 h period under the following reaction conditions: (1) pH, 4.5; (2) initial Se concentration, 0.025 mM; (3) clay concentration, 0.5 g/L; (4) temperature, 298 K; (5) background electrolyte, 0.01 M $NaNO_3$; and (6) initial reaction volume, 200 mL. Sodium selenite (Na_2SeO_3) salt solution with pH 4.5 was always used for adsorption equilibration. One hundred milligrams of a clay specimen were added to a 500 mL Pyrex Erlenmeyer flask carrying 170 mg of $NaNO_3$ dissolved in 180 mL of double-deionized water and mixed very well using a magnetic stirrer. The pH of the suspension was adjusted to pH 4.5 using 0.1 M HNO_3 or 0.1 M NaOH. The suspension was then shaken for 24 h in a constant-temperature water bath with periodic adjustments of pH to 4.5. After this 24 h shaking, the suspension pH was readjusted to 4.5 and the volume of water was adjusted to 195 mL by weighing the reaction vessel. A five-mL aliquot of 1.0 mM Na_2SeO_3 solution (pH 4.5) was then carefully added to the suspension under magnetic stirring and the reaction vessel was then immediately transferred to the constant temperature water bath and shaken for 24 h. After 24 h, the suspension was filtered through a 0.1 μm millipore membrane filter within 15 s using a vacuum facility. The pH and Se concentration in the filtrates were determined. The amount adsorbed was determined from the difference between the concentration of Se in the solution that was initially added (0.025 mM) and that which remained in the filtrate.

The separated solid phase on the membrane filter was then washed with 50 mL of double-deionized water five times (thus, a total of 250 mL double-deionized water was used for washing) to remove the free Se-containing entrained solution. The filtrates were saved separately for later determination of Se. The water-washed solid phase along with the membrane filter was transferred to a 500 mL Pyrex Erlenmeyer flask carrying 200 mL of a desorbing solution preadjusted to pH 4.5. The different desorbing solutions used in this study were: 0, 5×10^{-6}, 5×10^{-5} and 5×10^{-4} M citric acid in 0.01 M $NaNO_3$. After an immediate resuspension of the solid phase in the desorbing solution by hand shaking, the reaction vessel was quickly transferred to the constant-temperature water bath and shaken at 298 K. At various times (0.25, 0.5, 1.0, 1.5, 2.0, 3.0, 5.0, 8.0, 16.0, and 24.0 h) between 0.25 and 24 h, a 15 mL aliquot of the suspension was withdrawn from the system and filtered through a 0.1 μm millipore membrane filter within 15 s using a vacuum facility. The pH and Se concentration in the filtrates were determined and the amount of Se desorbed after a particular reaction period calculated.

To evaluate the heat of activation and the pre-exponential factor involved in the citrate-induced Se desorption from different clay systems, the kinetic experiments as described above were conducted at different temperatures of 288, 298, 308, and 318 K using 5×10^{-6} M citric acid in 10^{-2} M $NaNO_3$ (pH 4.5) as the desorbing solution.

Determination of Se was carried out by hydride generation atomic absorption spectrometry (HGAAS) as described by Huang and Fujii (1996). The system used a Varian VGA-77 continuous-flow hydride generator (Varian Australia Pty Ltd) coupled to a Spectra AA-220 AAS (Varian Australia Pty Ltd). Freshly prepared 0.6% (w/v) sodium borohydride solution and 7 M HCl were used for hydride vapor generation by the VGA apparatus. The method had a detection limit of 1.27×10^{-8} M. After adsorption and desorption equilibrium, KBr pellet IR absorption patterns of the freeze-dried clay specimens were recorded following the same method as stated earlier.

Fitting the rate equations and statistical analyses

The linear forms of different kinetic and empirical equations were applied to the desorption data and their goodness of fit was evaluated based on the r^2, standard error (SE), and level of significance (p) values. Instead of the amounts of Se released to the solution or remaining adsorbed per unit mass of the clays after different reaction periods, the mole fractions of pre-adsorbed Se released to the solution or remaining adsorbed onto the clay surfaces were used to fit the rate equations. This approach allowed a rigorous comparison of the relative bonding strengths of Se onto the surfaces of different clays when they had different amounts of pre-adsorbed Se on their surfaces. The comparisons of the mole fractions of pre-adsorbed Se desorbed, and desorption rate parameters in different systems were obtained using a least significant difference (LSD) test. The LSD values were calculated based on SE and t values at appropriate degrees of freedom at 95 and 99% confidence levels. The LSD values for the rate coefficient parameter were calculated based on the standard errors of the estimated rate parameters of the desorption-rate equation concerned. The LSD values for the heat of activation (E_a) were calculated based on the standard errors of the slopes for the Arrhenius equation plots. The LSD values for the pre-exponential factor (A) were calculated based on the standard error of the intercept of the lines obtained from the plots of Arrhenius equation.

RESULTS AND DISCUSSION

Characteristics of the adsorbents

A larger amount of Al was adsorbed on Mt from the HAS solution than from the HyA solution (Table 1). The estimated OH/Al ratios (according to Hsu, 1968) of both HyA and HAS materials adsorbed on Mt were around 2.7 (Table 1), the same as the ratio calculated for a variety of preparations by Barnhisel and Bertsch (1989). The parent HAS solution used to prepare the HAS-Mt complex had a Si/Al molar ratio of ~1.00 (Table 1). Thus, we do not rule out the possibility of the formation of a mixture of HAS_A and HAS_B in the parent HAS solution. However, the molar ratio of the Si/Al adsorbed on Mt was 0.48 (Table 1), suggesting that HAS_A was preferentially adsorbed on Mt. The FTIR absorption band at 940 cm^{-1} as observed in the solid phase of the HAS-Mt system (discussed below) also indicates that HAS_A was the dominant species adsorbed on Mt.

Both HyA and HAS interlayerings/coatings on Mt resulted in a significant reduction in CEC contributed by permanent negative charge and a substantial increase in that contributed by pH-dependent negative charge (Table 1). However, the CEC of the HAS-Mt complex exhibited weaker pH-dependence than that of the HyA-Mt. The PZSE values for the HAS-Mt complex (4.4) were slightly lower than that of the HyA-Mt (4.7). The adsorption of HyA or HAS on Mt reduced the total and internal surface areas and increased the external surface area to a substantial extent (Table 1). The charge and surface characteristics of these complexes are in good agreement with those reported by Inoue and Satoh (1993) and Sakurai and Huang (1998).

The K-saturated HyA/HAS-Mt complexes had an expanded d_{001} spacing (1.47−1.82 nm) in comparison to Mt (1.22 nm), suggesting that at least some of the HyA/HAS polymers were fixed in the interlayer (data not shown). The synthesized HyA and HAS-interlayers showed a considerable thermal stability when heated at 383 and 573 K. This is consistent with the behavior observed for most preparations of hydroxy interlayered smectites (Harsh and Doner, 1984).

Mole fraction of pre-adsorbed Se released

Of 50 mmoles of Se added per kg of clay, the untreated Mt in 24 h adsorbed only ~11%. In sharp contrast, the percentages of added Se adsorbed on HyA-Mt and HAS-Mt after 24 h were ~45% and 28%, respectively. In our previous study, Se adsorption kinetics on these clays also showed a faster adsorption on HyA-Mt followed by that on HAS-Mt and Mt (Saha *et al*., 2004).

The adsorption data stated above clearly show that the amounts of pre-adsorbed Se per unit mass of different clays were distinctly different from each other. Therefore, desorption results should be expressed in terms of the mole fraction (or % on a molar basis) of pre-adsorbed Se released rather than the amount of Se released per unit mass of the clays; this means of expression brings all the clays to a common basis. Thus, it would measure the relative ease of the release of Se pre-adsorbed in different clay systems, which would in turn be related to the relative adsorption bond strength of Se (Saha *et al*., 2005). This should be equally applicable to the comparison of the degree of fit of kinetic models to the data and the rate coefficients of Se released from various clay systems.

Washing the Se-sorbed solids with H_2O yielded little release of Se in all three clay systems. In the filtrate evolved from the first step of washing, the Se content was >100 times more dilute than that in the solution collected after the adsorption equilibrium; the Se content in the subsequent filtrates continued this trend and fell below the detection limit from the third washing onward.

The time-functions of citrate-induced Se desorption from various clay systems at 298 K are shown in Figure 1. The results showed a typical pattern of a rapid initial release of Se followed by a slowing down of the release rates and attainment of a final equilibrium. All the desorption systems invariably reached an apparent equilibrium with respect to Se desorption by the end of the 24 h reaction period. Generally, the Se desorption occurred rapidly in the 0.25 to 2 h period and more slowly in the 2−16 h reaction period, indicating that Se adsorption consisted of a multiple rate process (Figure 1). Therefore, based on the steepness of the desorption curves, the reaction kinetics for Se desorption were divided into an initial fast reaction (0.25−2 h) followed by a slow reaction (2−16 h). The multiple rate characteristics of Se desorption may be related to the heterogeneity of the adsorption sites. Site heterogeneity is believed to result from the different accessibility of surface pores and sites with different adsorption affinity and binding strength (Benjamin and Leckie, 1981; Madrid and de Arambarri, 1985; Liu and Huang, 2000).

As stated previously, the amounts of Se adsorbed on the three clays were significantly different, the greatest being on HyA-Mt followed by HAS-Mt and Mt. In contrast, the mole fractions of pre-adsorbed Se released (represented by % Se desorbed on a mole-fraction basis in Table 2) in 24 h from HyA-Mt and HAS-Mt by different levels of citrate were 4−6 and 2−3 times lower than that released from Mt, respectively (Table 2). Such a clear opposite trend between the amounts adsorbed and the mole fractions desorbed indicates that HyA- and HAS-interlayering and coatings not only augmented the Se adsorption affinity and capacity of Mt, but also increased the strength of adsorption.

When the citrate level in the desorbing solution was increased from 0 to 5×10^{-4} M (*i.e.* 0 to 1000 mmole/kg clay), there was a concomitant increase (3- to 4-fold in the cases of different clays) in the mole fraction of pre-adsorbed Se released in 24 h (Table 2).

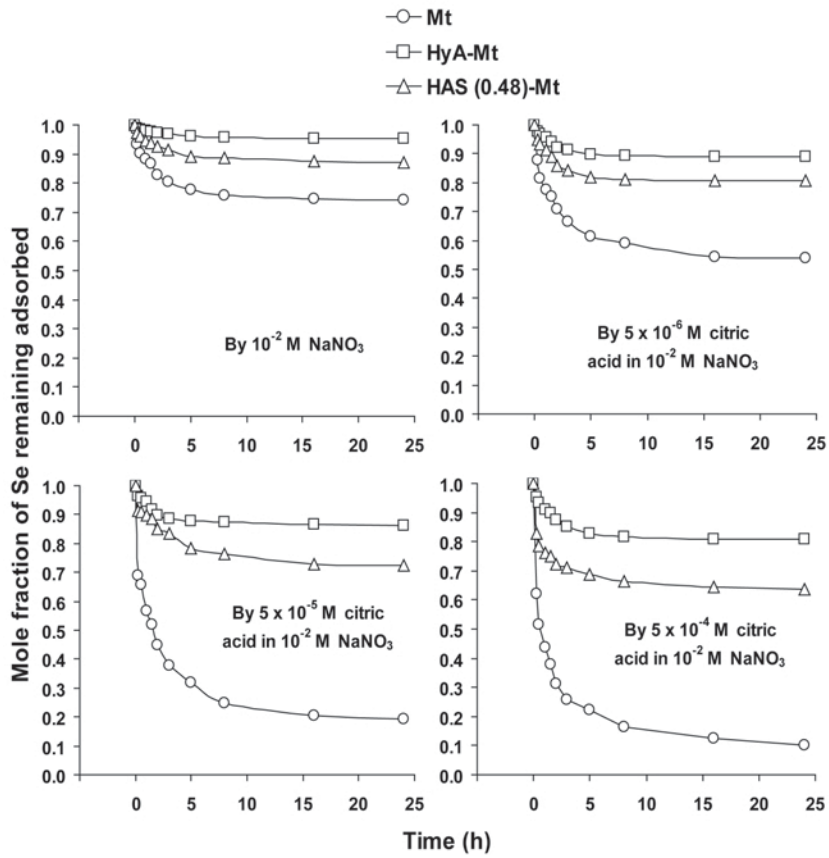

Figure 1. Time functions of citrate-induced Se desorption from montmorillonite as influenced by hydroxyaluminum and hydroxyaluminosilicate interlayering and coating at 298 K. Desorption always followed a 24 h adsorption equilibration at 298 K with clay concentration of 0.5 g L^{-1}; initial pH of 4.5; intial Se concentration of 0.025 mM; and background electrolyte of 10^{-2} M $NaNO_3$.

Application of kinetic and empirical models

Linear forms of different kinetic and empirical equations, including the zero-, first- and second-order rate equations, the power function (modified Freundlich), Elovich, and the parabolic diffusion equations were applied to the Se desorption data. The goodness of fit of the equations to the data was evaluated by using the correlation coefficient (r^2), standard error (SE), and probability (p) of linear regression analysis. That means a higher r^2 value coupled with lower SE and p values indicate a better fit. Consideration of a dual rate rather than a single rate characteristic of Se desorption kinetics, in each desorption system, invariably improved the goodness of each of the six models applied to our data (data not shown). All of the six models described the kinetics of Se desorption data reasonably well (the p values for individual kinetic data are not shown). This is consistent with the existing literature dealing with heterogeneous systems where it has often been shown that a number of kinetic and empirical models seem to describe satisfactorily the adsorption-desorption rate data (Chien and Clayton, 1980; Sparks and Jardine, 1984). The goodness of fit for various models in the present study was evaluated based on the mean values of r^2, SE and p (Table 3) obtained by applying different models to the individual kinetic data as described in the footnote of Table 3. For the fast reaction, the second-order rate equation had the highest mean r^2 associated with the lowest mean SE and p values (Table 3), suggesting an overall best fit of the second-order rate equation to the fast reaction kinetics. In contrast, the slow reaction kinetics of Se desorption were, in general, best described by the Elovich model which was followed by power-function and parabolic diffusion models. Among the three ordered models, the second-order rate equation, however, best described slow reaction kinetics of Se desorption based on the mean values of r^2, SE and p values (Table 3).

Considering all these observations, a multiple second-order rate equation was chosen as a common model in this study to compare the rates of Se desorption for both fast and slow reactions under different experimental conditions, even though the Elovich model appeared as the best in describing the slow reaction kinetics. However, the parameters derived by the Elovich model

Table 2. Citrate-induced desorption pattern of presorbed Se from Mt, HyA-Mt and HAS-Mt at 298K[a].

Desorbing solutions (molarity of citric acid in 10^{-2} M $NaNO_3$)	Clays					
	Mt	HyA-Mt	HAS Mt	CV (%)	$LSD_{0.05}$	$LSD_{0.01}$
	% Se desorbed after 24 h (on a mole-fraction basis)					
0	24.1dA	4.8dC	12.7dB	4.5	2.0	3.6
5×10^{-6}	45.5cA	10.9cC	19.5cB	3.2	2.6	4.7
5×10^{-5}	85.1bA	13.7bC	28.1bB	3.9	5.3	9.7
5×10^{-4}	92.0aA	19.6aC	35.9aB	6.1	9.5	17.4
CV (%)	3.3	5.1	4.4			
$LSD_{0.05}$	5.7	1.7	3.0			
$LSD_{0.01}$	9.5	2.9	4.9			

[a] Desorption always followed a 24 h adsorption equilibration at 298 K with clay concentration of 0.5 g L^{-1}; initial pH of 4.5; intial selenite concentration of 0.025 mM; and background electrolyte of 0.01 M $NaNO_3$. The amounts of Se adsorbed by Mt, HyA-Mt, HAS-Mt at the end of the 24 h reaction period were 5.72, 22.25 and 13.86 mmole kg^{-1}, respectively. Figures in a column followed by same lower case letter(s) do not differ significantly at 5% level of significance; figures in a row followed by same upper case letter(s) do not differ significantly at 5% level of significance; for comparison within a column, disregard the upper case letter(s) following the values; for comparison within a row, disregard the lower case letter(s) following the values.

are not well defined physicochemically and the equation may not provide a real rate constant (Bolan *et al.*, 1985). Hence, the parameters of the Elovich equation would not give a fair estimation of activation energy (E_a) and pre-exponential factor (A) of Se desorption from the clays based on the Arrhenius equation. As the second-order rate equation performed best among all six models tested in describing the fast reaction kinetics and it also appeared as the best among the three ordered models in describing the slow reaction kinetics, adopting this as a common model to characterize the desorption rates is logically sound. Further, temperature dependence of the

Table 3. Summary of the mean values of r^2, standard error (SE), and p for different kinetic models fitted to the data[a].

Model	Se desorption from various clay systems by four different citric acid concentrations (*i.e.* 0, 5×10^{-6}, 5×10^{-5}, and 5×10^{-4} M citric acid in 10^{-2} M $NaNO_3$) at 298 K			Se desorption from various clay systems by 5×10^{-6} M citric acid in 10^{-2} M $NaNO_3$ at four different temperatures (*i.e.* 288, 298, 308, and 318 K)		
	r^2	SE	p	r^2	SE	p
Fast reaction (0.25−2 h)						
Zero-order	0.9625	9.4×10^{-3}	3.8×10^{-3}	0.9619	1.1×10^{-2}	4.1×10^{-3}
First-order	0.9671	8.3×10^{-3}	3.1×10^{-3}	0.9650	1.0×10^{-2}	3.6×10^{-3}
Second-order	0.9688	8.1×10^{-3}	2.9×10^{-3}	0.9664	9.9×10^{-3}	3.4×10^{-3}
Power function	0.9644	8.4×10^{-3}	4.2×10^{-3}	0.9620	1.0×10^{-2}	4.2×10^{-3}
Elovich	0.9320	1.0×10^{-2}	1.0×10^{-2}	0.9247	1.2×10^{-2}	1.1×10^{-2}
Parabolic diffusion	0.9626	8.3×10^{-3}	4.1×10^{-3}	0.9585	1.0×10^{-2}	4.6×10^{-3}
Slow reaction (2−16 h)						
Zero-order	0.8757	1.7×10^{-2}	2.1×10^{-2}	0.8749	1.6×10^{-2}	2.1×10^{-2}
First-order	0.8602	1.7×10^{-2}	2.4×10^{-2}	0.8881	1.5×10^{-2}	1.8×10^{-2}
Second-order	0.8772	1.5×10^{-2}	2.0×10^{-2}	0.9004	1.4×10^{-2}	1.5×10^{-2}
Power function	0.9601	9.3×10^{-3}	3.5×10^{-3}	0.9627	8.3×10^{-3}	3.3×10^{-3}
Elovich	0.9772	6.9×10^{-3}	1.5×10^{-3}	0.9669	6.8×10^{-3}	3.3×10^{-3}
Parabolic diffusion	0.9222	1.3×10^{-2}	9.6×10^{-3}	0.9360	1.1×10^{-2}	7.6×10^{-3}

[a] Desorption always followed a 24 h adsorption equilibration under conditions stated in the footnotes of Table 2. For any kinetic model, the mean values presented here were derived from the individual values obtained through applying the model separately to the 12 individual kinetic data under each of the two separate groups: (1) three clay systems and four citric acid concentrations (*i.e.* 0, 5×10^{-6}, 5×10^{-5}, and 5×10^{-4} M citric acid in 10^{-2} M $NaNO_3$) at 298 K; and (2) three clay systems and four temperatures (*i.e.* 288, 298, 308, and 318 K) with 5×10^{-6} M citric acid in 10^{-2} M $NaNO_3$. This summary table is used to show the mean values of r^2, p and SE at a glance for the kinetic data under the two aforementioned groups.

second-order rate coefficient allows a fair estimation of E_a and A based on the Arrhenius equation. As examples, the actual plots of the second-order rate equations for the desorption systems at 298 K are shown in Figure 2.

Despite the reported mechanistic implications of the best fit of a particular model to some sorption-desorption kinetic data involving soils and clays (Low, 1960; Hingston, 1981), it should be noted that there is no valid relationship between the equation that gives the best fits and the physicochemical and mineralogical properties of the adsorbents being studied (Sparks, 2003). There is no correlation between the applicability of any of these equations and the nature of the processes actually involved; dissimilar processes are often fitted by the same equation and similar processes are fitted by different equations (Aharoni and Sparks, 1991). Nevertheless, the parameters of the chosen model(s) do provide some meaningful tools for comparison of the rates of adsorption or desorption processes on or from different adsorbents.

Rates of Se desorption

As discussed in the preceding section, the second-order rate constant was used as a tool to compare the Se desorption rates in different adsorption systems. The second-order rate equation in our case is: $1/Q_t = 1/Q_0 + kt$, where Q_t = mole fraction of selenite remaining adsorbed after the desorption period, t (h); Q_0 = mole fraction of selenite remaining adsorbed before desorption = 1; k = desorption rate constant. The values of the second-order rate constant (k) for the 12 desorption systems comprising three different clays and four different citric acid concentrations at 298 K are given in Table 4. Depending on the concentration of citric acid in the desorbing solutions, the fast reaction apparently had 2−7, 5−14, and 5−8 times greater desorption rates than the respective slow reaction for Mt, HyA-Mt and HAS-Mt, respectively. For both fast and slow reactions, Se desorption rates were significantly different for different clays in the order Mt >> HAS-Mt > HyA-Mt for all the citric acid concentrations except for the fast reaction with 5×10^{-5} M citric acid in 10^{-2} M $NaNO_3$ where there was no significant difference between HyA-Mt and HAS-Mt. In general, elevated concentrations of citric acid in the desorbing solution brought about a significant enhancement in the remobilization rates of pre-adsorbed Se in the cases of both fast and slow reactions.

Temperature effects on Se desorption

The effects of temperature on the time-function of 5×10^{-6} M citrate-induced Se desorption from the clays are shown in Figure 3. Temperature exerted a noticeable influence on the time-function of Se desorption from all three clay systems, with an increased extent of desorption taking place with elevated temperature at any particular time.

Figure 4 shows the effects of temperature on the second-order rate constant (k) of citrate-induced Se desorption from different clays. Elevated temperature increased the k values of both fast and slow reactions for different desorption systems. As revealed by the slope of the regression lines in Figure 4, temperature effects on the k value were more pronounced for the stronger adsorbent, *i.e.* HyA-Mt > HAS-Mt > Mt; and this was true for both fast and slow reactions, suggesting that more energy would be required for the desorption from a stronger adsorbent. Generally, the rate constants for both fast and slow reactions of Se desorption from various clay systems followed the trend Mt > HAS-Mt > HyA-Mt at any given temperature with two exceptions; for the fast reaction at 308 and 318 K, HyA-Mt had greater rate constants than HAS-Mt (Figure 4). As mentioned above, the data indicate that the Se desorption from HyA-Mt is more temperature dependent than HAS-Mt. This is also reflected in the higher heat of activation for Se desorption from HyA-Mt compared with HAS-Mt as discussed in the succeeding section.

Activation energy and pre-exponential factors for desorption

Figure 4 shows the Arrhenius plots for the Se desorption from different clay systems. All the plots for the fast reaction yielded a significant linear relationship with r^2 values ranging from 0.8839 to 0.9906 and $p < 0.06$ (Figure 4). The plots for the slow reaction, however, had r^2 in the range of 0.8307 to 0.9933 with $p < 0.09$. The values of the activation energy (E_a) and pre-exponential factor (A) are given in Table 5. The E_a is the Arrhenius activation energy which must be overcome before desorption of Se can take place. The A is a measure of the frequency of collision of the reactant (desorbing agent) with the reactive sites on the clay surface carrying adsorbed Se. For both fast and slow reactions, the E_a values of Se desorption were significantly different for the three clay systems: HyA-Mt >> HAS-Mt > Mt. Such results strengthened the basis of the inference that HyA/HAS interlayering and coatings on Mt increased the Se adsorption bond strength to a significant extent, thus requiring more energy for the desorption process. The E_a of a diffusion-controlled process in solution is ~25 kJ mol^{-1} (Sparks, 1999). However, in heterogeneous systems such as mineral-water interfaces, diffusion occurs not only in the bulk solution but also in micropores and macropores, in the films around solid particles, on the solid surface, and inside solid particles (Sparks, 1989). Therefore, the E_a for diffusion-controlled processes in heterogeneous systems is greater than that in solutions. Film diffusion typically has an E_a of 17−21 kJ mol^{-1} and intraparticle diffusion has E_a values of 21−42 kJ mol^{-1} (Sparks, 1999). Thus, low $E_a$values (<42 kJ mol^{-1}) indicate diffusion-controlled processes whereas higher $E_a$values (>42 kJ mol^{-1}) indicate chemically controlled processes (Sparks, 1989). Therefore, the data indicate that the rate-limiting steps in the fast reactions of Se desorption from

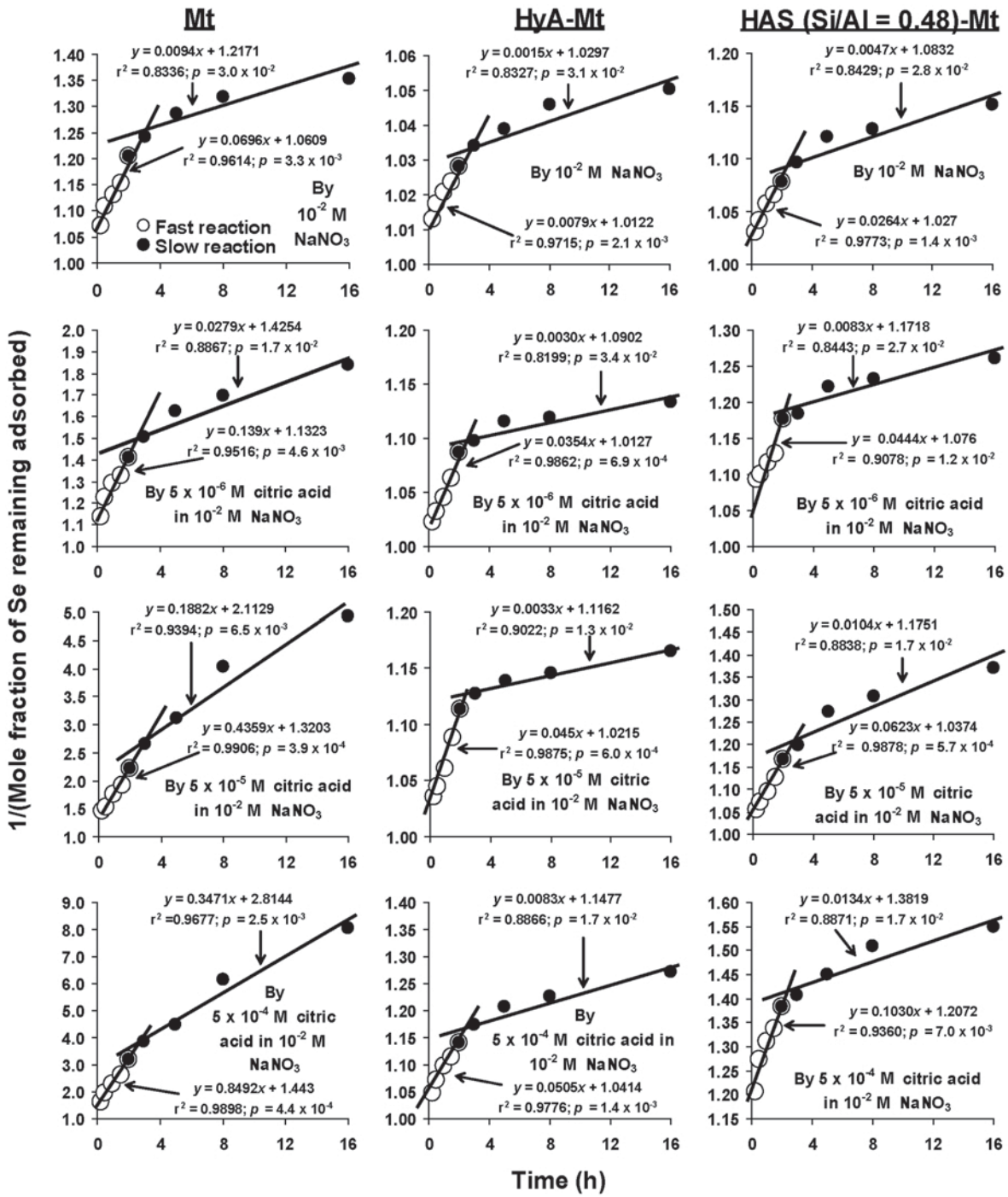

Figure 2. Fitting second-order rate equation on Se desorption kinetics in various clay and desorption systems at 298 K. Study of desorption kinetics followed a 24 h adsorption reaction conducted under the conditions described in the caption of Figure 1.

Mt and HAS-Mt are diffusion-controlled process. The E_a for the fast reaction of Se desorption from HyA-Mt is >>42 kJ mol^{-1}, indicating that the rate-limiting step in this case is a chemically-controlled process (Table 5). On the other hand, the rate-limiting steps in the slow reactions of Se desorption from all the three clay systems are diffusion-controlled processes.

Desorption of a smaller mole fraction of the pre-adsorbed Se after a particular reaction period (Figure 1), slower kinetics (Table 4), and a greater E_a of desorption (Table 5) all suggest an increased bond strength of Se adsorption to the clays. Thus, both HyA- and HAS-interlayerings/coatings on Mt definitely rendered a stronger Se adsorption on the resultant surfaces. This

Table 4. Rate parameters of the second-order model applied to data of the kinetics of Se desorption from Mt, HyA-Mt and HAS-Mt at 298 K[a].

Desorbing solution (Mmolarity of citric acid in 10^{-2} M $NaNO_3$)	Second-order rate constant[b] (Mole fraction^{-1} h^{-1}) $\times 10^3$					
	Mt	HyA-Mt	HAS-Mt	CV (%)	$LSD_{0.05} \times 10^3$	$LSD_{0.01} \times 10^3$
Fast reaction						
0	70aC	8A	26aB	2.5	4	9
5×10^{-6}	139bC	35bA	44bB	2.8	9	21
5×10^{-5}	436cB	45cA	62cA	5.0	39	90
5×10^{-4}	849dC	51dA	103dB	1.2	17	19
CV (%)	3.2	4.3	4.0			
$LSD_{0.05} \times 10^3$	38	5	8			
$LSD_{0.01} \times 10^3$	70	9	14			
Slow reaction						
0	9aC	1aA	5aB	6.7	2	4
5×10^{-6}	28bC	3bA	8bB	5.6	3	7
5×10^{-5}	188cC	3bA	10cB	3.8	1	3
5×10^{-4}	347dC	8cA	13dB	4.3	2	5
CV (%)	3.2	5.6	5.8			
$LSD_{0.05} \times 10^3$	15	1	2			
$LSD_{0.01} \times 10^3$	27	1	3			

[a] Based on 16 h desorption kinetics (a fast reaction from 0.25 to 2 h followed by a slow reaction from 2 to 16 h). Desorption always followed a 24 h adsorption equilibration under conditions stated in the footnotes of Table 2. Figures in a column followed by same lower case letter(s) do not differ significantly at 5% level of significance; figures in a row followed by same upper case letter(s) do not differ significantly at 5% level of significance; for comparison within a column, disregard the upper case letter(s) following the values; for comparison within a row, disregard the lower case letter(s) following the values.
[b] The second-order rate constant, and their LSD values denoted in the table should be multiplied by 10^{-3}.

is, in part, attributed to the added positively charged surfaces on Mt as revealed by the reduced CEC and measurable PZSE of the HyA/HAS-Mt complexes relative to untreated Mt (see Table 1). An electrostatic attraction of the negatively charged Se ions to the positively charged surface functional groups ($Al\text{-}OH_2^+$) forming outer-sphere surface complexes ultimately leads to strong adsorption as inner-sphere surface complexes (Hingston *et al.*, 1972; Dynes and Huang, 1995; Schulthess and Hu, 2001).

It has been shown that the edge surfaces [$Al\text{-}(H_2O)(OH)$] of gibbsite are much more reactive than its (001) faces (Al-OH-Al hydroxyls) (Parfitt *et al.*, 1977). However, the poorly ordered HyA polymers are expected to have substantial structural defects on their (001) faces and the Al-OH groups after protonation around these defect sites would be as reactive as their edge counterparts. In HAS ionic solution, the $Si(OH)_4$ molecules would be complexed through the reaction of Si-OH groups with the $Al\text{-}OH/OH_2$ groups at the edges and defect sites of the HyA ions, reducing the frequency distribution of Al-OH or $Al\text{-}OH_2$ groups on these sites (Wada and Wada, 1980; Sterte and Shabtai, 1987). Consequently, silication of HyA ions would reduce their

Table 5. Activation energy and pre-exponential factor values of Se desorption by 5×10^{-6} M citric acid in 10^{-2} M $NaNO_3$ from Mt, HyA-Mt and HAS-Mt[a].

Sample	Fast reaction		Slow reaction	
	Activation energy (kJ mole^{-1})	Pre-exponential factor (Mol fraction^{-1} h^{-1})	Activation energy (kJ mole^{-1})	Pre-exponential factor (Mol fraction^{-1} h^{-1})
Mt	22a	1.3×10^3a	11a	2.3×10^0a
HyA-Mt	74c	4.4×10^{11}b	35c	6.8×10^3b
HAS-Mt	32b	3.1×10^4a	22b	7.7×10^1a
CV (%)	4.40	4.86	4.58	5.90
$LSD_{0.05}$	8	3.0×10^{10}	5	5.8×10^2
$LSD_{0.01}$	19	7.0×10^{10}	10	1.3×10^3

[a] Based on 16 h desorption kinetics (a fast reaction from 0.25 to 2 h followed by a slow reaction from 2 to 16 h). Desorption always followed a 24 h adsorption equilibration under conditions stated in the footnotes of Table 2. Figures in a column followed by same letter(s) do not differ significantly at 5% level of significance.

reactivity to Se. Relative to HyA-Mt, a significant reduction in the bond strength of Se adsorption on a HAS-Mt complex, as revealed by a greater mole fraction desorbed after a particular reaction period, faster kinetics, and a lower E_a of desorption (see Tables 2, 4 and 5) support the reasoning.

The value of A for both fast and slow reactions in the cases of different clays followed the order HyA-Mt >> HAS-Mt >> Mt (Table 5), exactly the same as the order of the amount of Se adsorbed per unit mass (footnote of Table 2). This is very logical in the sense that when the reactive sites with adsorbed Se on the clay surface are more abundant, the frequency of collision of citrate with these sites (*i.e.* A) would be greater.

Furthermore, the results show that the fast reaction of Se desorption required a greater E_a than the slow reaction (Table 5). The Arrhenius equation (as stated earlier) indicates that the rate constant of Se desorption at a constant temperature is as a function of both E_a and A. Therefore, A plays an important role in influencing the reaction rate. In the fast reaction, although Se might be bound relatively tightly to the reaction sites and needed more energy to break the bond to release selenite, the frequency of collision of citrate with Se adsorbed on the reactive sites was much greater in the fast reaction compared with the slow reaction, since more Se was present on the surfaces at the early stage of the reaction. As a result, Se desorption occurred at a greater rate at the early stage of the reaction even though the E_a was relatively high. As the Se concentration on the surfaces gradually decreased with the reaction time, the desorption rate became slower, principally due to lower collision frequency (A). At this stage, some of the Se adsorbed may be present at the sites which take longer to reach by the desorbing agent through diffusion process, but the energy required to release Se may be low once citrate collides with adsorbed Se.

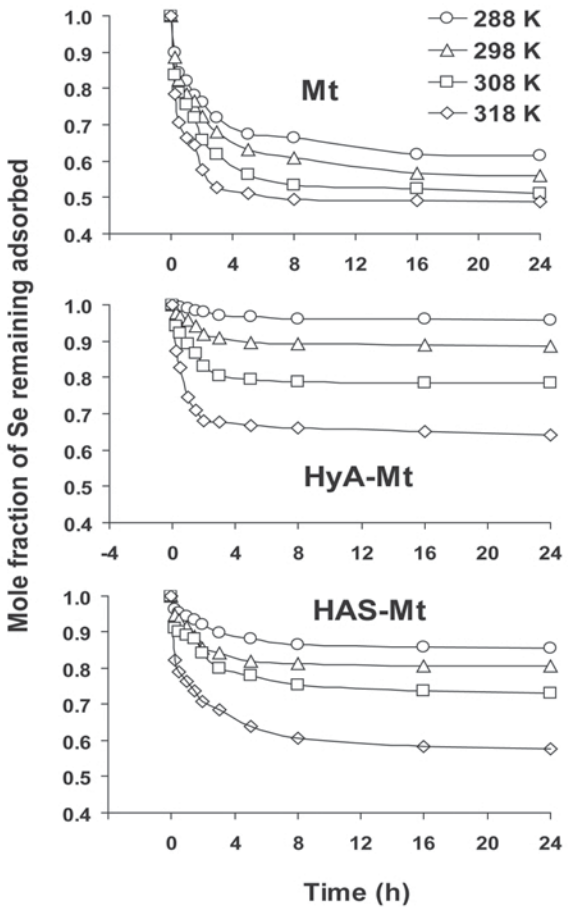

Figure 3. Temperature effects on the time-functions of citrate-induced (by 5×10^{-6} M citric acid in 10^{-2} M $NaNO_3$) Se desorption from montmorillonite as influenced by hydroxy-aluminum and hydroxyaluminosilicate interlayering and coating. Study of desorption kinetics followed a 24 h adsorption reaction conducted under the conditions described in the caption of Figure 1.

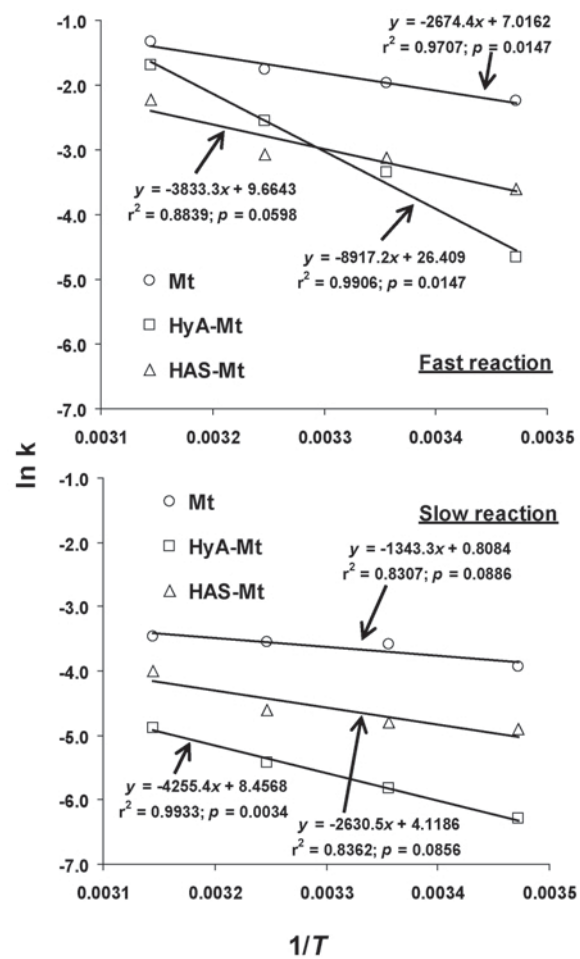

Figure 4. Arrhenius plots of the kinetics of Se desorption by 5×10^{-6} M citric acid in 10^{-2} M $NaNO_3$, where k is the second-order rate constant (mole fraction^{-1} h^{-1}) and T is absolute temperature (K).

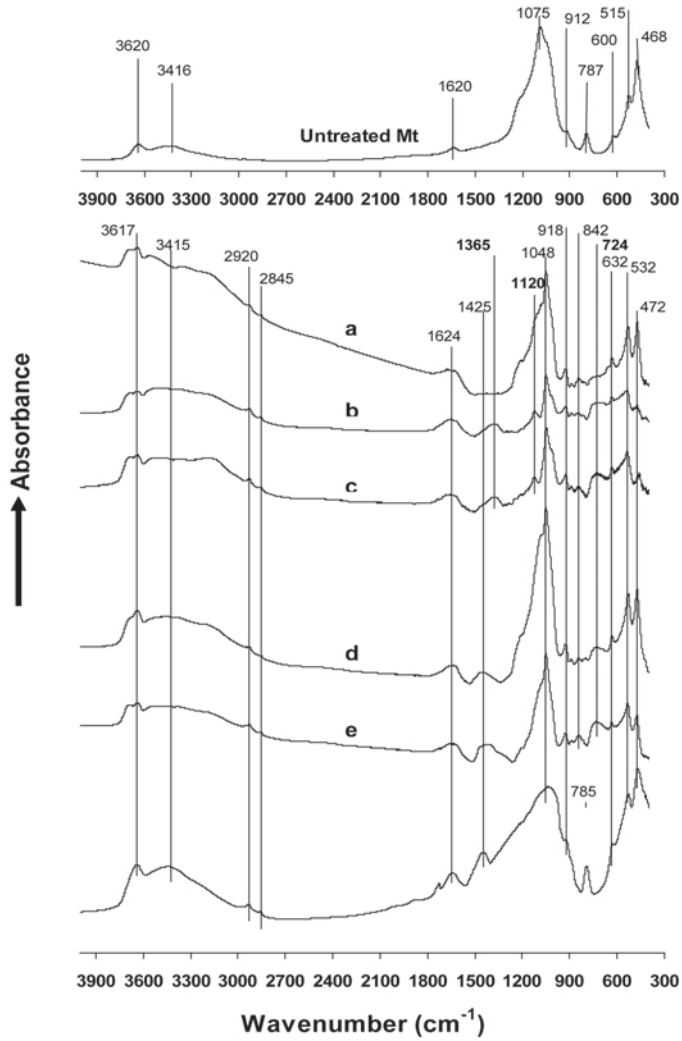

Figure 5. FTIR spectrum of untreated Mt (the top most one), and difference FTIR spectra after subtraction of the spectrum of untreated Mt (without adsorbed Se) from that of HyA-Mt for different conditions: (a) before adsorption of Se; (b) after adsorption of Se; (c) after desorption of pre-adsorbed Se by 0.01 M $NaNO_3$; (d) after desorption of pre-adsorbed Se by 5×10^{-6} M citric acid in 10^{-2} M $NaNO_3$; (e) after desorption of pre-adsorbed Se by 5×10^{-5} M citric acid in 10^{-2} M $NaNO_3$; (f) after desorption of pre-adsorbed Se by 5×10^{-4} M citric acid in 10^{-2} M $NaNO_3$.

IR absorption patterns of the clays before and after sorption-desorption

The FTIR spectrum of untreated Mt (Figures 5 and 6) exhibits the major IR absorption bands at 3620 cm^{-1} (Al-OH stretching), 3416 cm^{-1} (OH stretching of adsorbed water), 1610 cm^{-1} (OH bending of adsorbed water), and 912 cm^{-1} (Al-OH bending), which are very close to those reported by White and Roth (1986) and Sakurai and Huang (1998). The Si-O-Al and Si-O-Mg bending vibrations were observed at 515 and 468 cm^{-1}, respectively, which are very close to those reported by Lou and Huang (1994) and Sakurai and Huang (1998). The IR absorption bands at 1075, 787 and 600 cm^{-1} are attributed to the mineral cristobalite (Marel and Beutelspacher, 1976), which was present in the Mt as an impurity (Inoue and Satoh, 1993).

The IR absorption bands for the HyA and HAS ions adsorbed on Mt were resolved by analyzing the difference spectra between the HyA/HAS-Mt complexes and untreated Mt (see Figures 5 and 6). The IR absorption features of the adsorbed HyA ions (Figure 5, spectrum a) resemble that of hydrargillite (a gibbsite) (Marel and Beutelspacher, 1976). For the HAS-Mt complexes, the characteristic IR absorption band at 940 cm^{-1} arising from the Si-O stretching of the orthosilicate groups of the adsorbed HAS was clearly observed (Figure 6, spectrum a). This IR absorption band is a characteristic feature of proto-imogolite (Farmer *et al.*, 1979), a poorly ordered imogolite or a precursor of imogolite with a weakly developed incipient fibrosity (Farmer *et al.*, 1978).

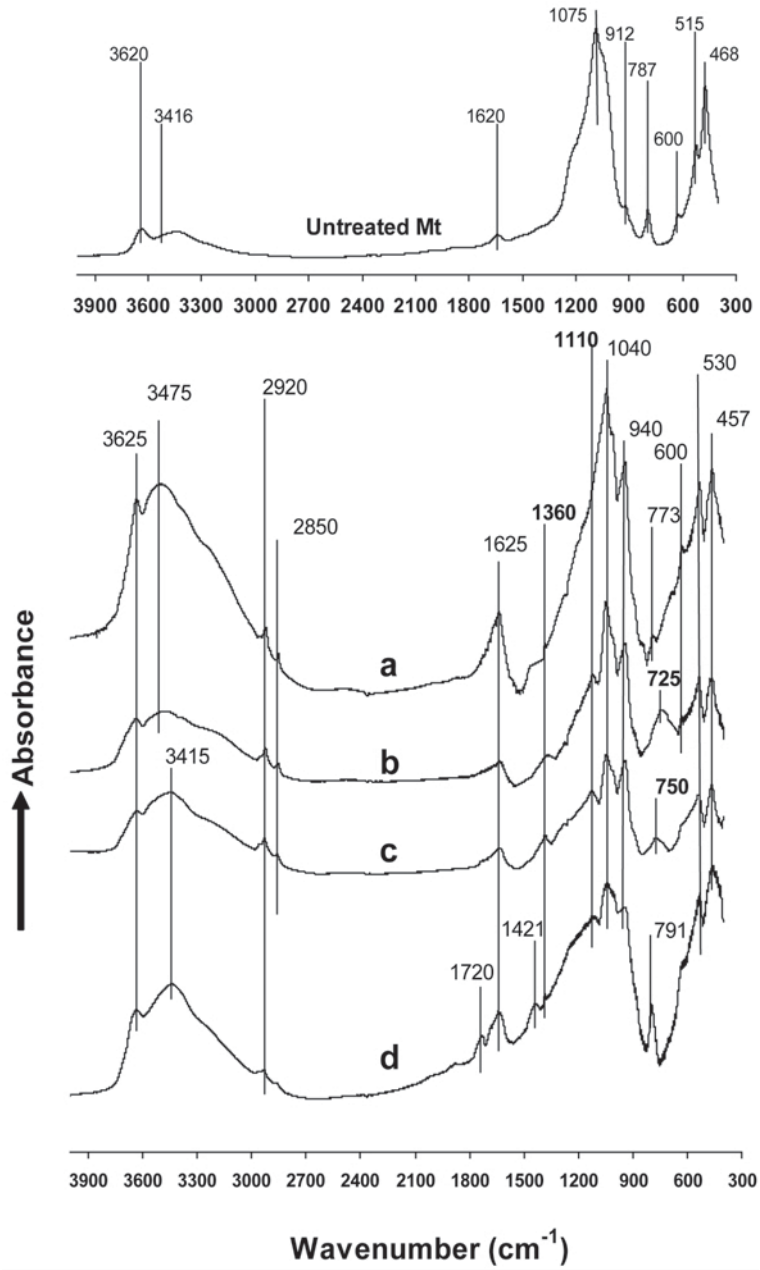

Figure 6. FTIR spectra of untreated Mt (the top-most one); and difference FTIR spectra after subtraction of the spectrum of untreated Mt (without adsorbed Se) from that of HAS(OH/Al = 2.0; Si/Al = 0.48)-Mt for different conditions: (a) before sorption of Se; (b) after sorption of Se; (c) after desorption of pre-adsorbed Se by 10^{-2} M $NaNO_3$; (d) after desorption of pre-adsorbed Se by 5×10^{-4} M citric acid in 10^{-2} M $NaNO_3$.

The difference FTIR spectra after subtraction of the spectrum of untreated Mt from that of HyA-Mt before and after adsorption of Se show the IR absorption bands at 724 and 1120 cm^{-1}, which are attributable to surface-adsorbed Se (Figure 5, comparison of spectra a and b). The FTIR spectra of both sodium selenite (Na_2SeO_3) and selenious acid (H_2SeO_3) generated in the present study (spectra not shown) and those found in the literature (Pouchert, 1985) also show a distinct IR absorption band between 700 and 850 cm^{-1}. Although the spectrum of selenious acid (H_2SeO_3) showed an IR absorption band in the region of 1110–1120 cm^{-1}, which is attributable to uncharged H_2SeO_3 (Nyquist and Kagel, 1971), that of sodium selenite (Na_2SeO_3) (Nyquist and Kagel, 1971) did not. The bands at 724 and 1120 cm^{-1} remained almost unchanged after carrying out a desorption step with 10^{-2} M $NaNO_3$ (Figure 5b and c), indicating little desorption of Se by nitrate. The IR absorption band at

1365 cm^{-1} in spectra b and c of Figure 5 is similar to that of $NaNO_3$ generated in the present study (not shown) and found in the literature (Pouchert, 1985).

Citrate even at the lowest concentration (5×10^{-6} M), when used as a desorbing agent, caused the disappearance of the IR absorption band of adsorbed Se at 1120 cm^{-1} (Figure 5, spectrum d). The band of adsorbed Se around 724 cm^{-1} disappeared only after desorption with the highest concentration of citrate (5×10^{-4} M) (Figure 5f). The appearance of the band at 785 cm^{-1}, which is attributed to selenite (Nyquist and Kagel, 1971), after the desorption with 5×10^{-4} M citrate (Figure 5f) appeared to be due to the removal of some of the adsorbed Se as indicated in the disappearance of the band at 724 cm^{-1} and the resultant appearance of the band at 785 cm^{-1} which was apparently masked by the broad band around 724 cm^{-1} before the 5×10^{-4} M citrate desorption treatment (Figure 5b, c, d, and e). The data indicate that the adsorbed Se as indicated by the band at 785 cm^{-1} is more strongly bound to the HyA and/or sterically inaccessible to citrate, and, thus, resistant to the desorption treatment of 5×10^{-4} M citrate (Figure 5f). As citrate resulted in a substantial desorption of Se, the absorption band of COO^- bending vibration of citrate ligand complexed with the clay surface became evident at 1425 and 1624 cm^{-1} (Figure 5d, e and f), which are similar to that reported for oxalate adsorbed to gibbsite (Parfitt *et al*., 1977) and Al hydroxides (Dynes and Huang, 1997). It should be noted that the band at 1624 cm^{-1} is also due to a HOH bending vibration of adsorbed water and hence it is common in all the spectra and found in spectra a, b and c of Figure 5 as well. In Figure 5f (after desorption of Se by 5×10^{-4} M citrate), the IR absorption band at 1721 cm^{-1} is due to a C=O bond of an undissociated COOH group (Inoue and Huang, 1984) of citric acid.

Figure 6 shows the difference FTIR spectra after subtraction of the spectrum of untreated Mt from that of HAS-Mt before and after sorption-desorption processes of Se. The common IR absorption band at 940 cm^{-1} is assigned to Si−O stretching of the adsorbed HAS ions because HAS polymers contain orthosilicate species (Lou and Huang, 1988, 1994). Based on the IR absorption spectra of selenious acid and selenite (Nyquist and Kagel, 1971; Pouchert, 1985; the data generated from pure chemicals in the present study), the IR absorption bands at 1110 cm^{-1} and between 725−791 cm^{-1} (Figure 6, spectra b, c, d) are attributable to surface-adsorbed, uncharged selenious acid and ionic selenite, respectively. The IR absorption band at 1110 cm^{-1} remained visible after desorption with nitrate and citrate (5×10^{-4} M) (Figure 6, spectra c and d), indicating that the uncharged selenious acid adsorbed as indicated by this IR absorption band is not replaceable by nitrate, and not accessible to citrate apparently due to steric hindrance to nanopores. The large broad band around 725 cm^{-1} shifted to the small narrow band around 750 cm^{-1} in the case of desorption with nitrate (Figure 6, spectrum c), indicating that the more loosely bound Se (outer-sphere surface complex) is replaced by nitrate. The band at ~750 cm^{-1} shifted to the sharper and narrow band at 791 cm^{-1} after desorption with 5×10^{-4} M citrate (Figure 6, spectrum d). This indicates that citrate treatment did not completely remove the adsorbed Se due to the bonding strength of Se to HAS and/or steric inaccessibility to nanopores. The present interpretations are substantiated by the IR absorption data of selenite in the range 725−791 cm^{-1} (Nyquist and Kagel, 1971).

The IR absorption spectroscopic evidence of surface-adsorbed Se and citrate on HyA-Mt (Figure 5a to 5f) and HAS-Mt (Figure 6a to 6d) surfaces, as discussed above,

Table 6. Release of Al and Si from Mt and HyA/HAS-Mt under different conditions at 298 K.

		Al and Si released after different treatments				
			After 24 h Se desorption equilibrium with different citric acid concentrations[b]			
Sample	Amount of Al and Si adsorbed before treatments (μmole g^{-1})	After 24 h Se sorption equilibrium[a]	10^{-2} M $NaNO_3$	5×10^{-6} M citric acid in 10^{-2} M $NaNO_3$	5×10^{-5} M citric acid in 10^{-2} M $NaNO_3$	5×10^{-4} M citric acid in 10^{-2} M $NaNO_3$
Al released (μmole g^{-1})						
Mt	0	0.0	0.0	9.6	20.8	39.8
HyA-Mt	1130	3.6	2.1	57.0	84.1	114.9
HAS-Mt	1370	7.2	3.3	87.6	124.8	159.3
Si released (μmole g^{-1})						
Mt	0	2.9	3.3	6.7	14.1	19.0
HyA-Mt	0	1.5	2.6	4.5	8.9	13.3
HAS-Mt	660	10.6	8.0	27.5	43.4	63.6

[a] Adsorption equilibration was conducted under conditions stated in the footnotes of Table 2.
[b] Desorption always followed a 24 h adsorption equilibration as stated above[a].

supports the contention that same adsorption sites were accessible to both citrate and Se. This suggests 'ligand exchange' as one of the mechanisms of citrate-induced desorption of Se from the HyA/HAS-Mt. It should be noted that because of the IR sampling technique followed in this study (KBr pellets prepared using freeze-dried samples), the situation after drying might deviate from the actual situation of the sorption-desorption phenomena, which occurred in the presence of water. Hence, the mechanistic interpretations of the types of bonding might have some limitations and merit future attention.

Amounts of Al and/or Si released

During Se desorption, there was concomitant release of Al or Al + Si to varying extents depending on the desorbing solution (Table 6). Greater amounts of Al and Si release took place when citrate + nitrate rather than nitrate alone was present in the desorbing solution. A further increase in Al and Si release occurred as the citrate concentration in the desorbing solution increased. However, the percentage of adsorbed Al and Si release (*i.e.* from HyA-Mt or HAS-Mt) never exceeded 12 and 10%, respectively, even under the greatest level of citrate. For HAS-Mt, the HAS ions had a Si/Al molar ratio of 0.48, while the base Mt has this ratio as 2.0. The molar ratio of Si to Al released by all the levels of citrate was even lower than that of HAS ions, indicating that dissolution took place predominantly on the complexing polymers rather than on the base Mt. That means the Al or Si in the complexing HyA/HAS ions are quite different from those in the structure of Mt with respect to their susceptibility to dissolution by citrate. Relative to untreated Mt, a smaller amount of Si released from the HyA-Mt in the cases of all the citric acid concentrations probably occurred due to the protection of the Si source (base Mt) by the HyA-coatings.

The r^2 values for the relationships between Se release *vs.* Al, Si or Al + Si released were significant at a 5% level in all cases, except for the Al and Al + Si release *vs.* Se release from Mt (Figure 7). This suggests that apart from the ligand-exchange mechanism as indicated by the FTIR data, discussed earlier, structural dissolution of the adsorbing surfaces is another mechanism of citrate-induced Se desorption in the present systems. For both Al and Al+Si release, the r^2 values were greater for HyA/HAS-Mt than Mt (Figure 7), suggesting that the structural dissolution mechanism could account for a greater proportion of the variation in the desorption data for the two complexes than base Mt. Besides citrate-induced ligand exchange and structural dissolution, another possible mechanism is that specific adsorption of citrate on the Se-free bare sites could increase the surface negative charge with a reduction in the PZSE of the surfaces, thus weakening the adsorption bond strength through electrostatic repulsion of the negative charge and inducing the release of surface adsorbed Se.

Even though there is no doubt that at least some of the Se desorption occurred through structural dissolution of the clays by citrate, the molar ratios of desorbed Se to the Al or Si released were low, ranging from 0.03 to 0.27 for Al and from 0.08 to 0.55 for Si. This is very logical in the sense that surface coverage by the adsorbed Se was very low; therefore, there were enormous Se-free potential sites; and the dissolution of Al or Al + Si might have occurred largely from the bare sites.

CONCLUSIONS

Hydroxy-interlayerings/coatings on expandable phyllosilicates in acidic soils and sediments is an inevitable and widely occurring pedogeochemical phenomenon that gives rise to HyA- and HAS-interlayered/coated Mt and Vt (vermiculite). This process has been

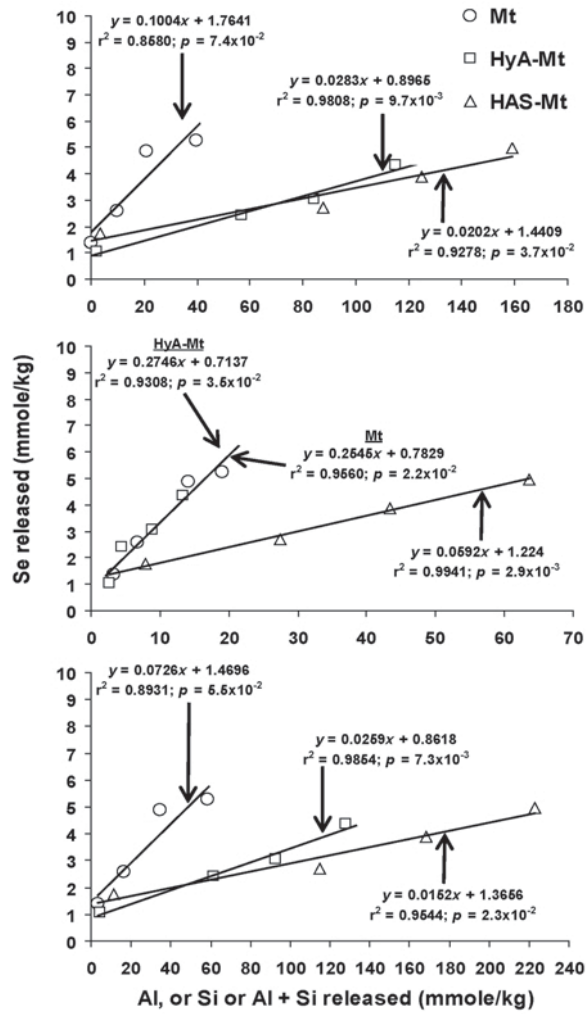

Figure 7. The relationships between Se released *vs.* Al, Si and Al+Si released after a 24 h of desorption equilibration with different citric acid concentrations (0, 5×10^{-6}, 5×10^{-5}, 5×10^{-4} M citric acid in 10^{-2} M $NaNO_3$) in Mt, HyA-Mt, and HAS-Mt systems at 298 K.

found to significantly alter the charge and surface properties of the parent Mt and Vt and hence it must have a tremendous influence on their interfacial reactions with plant nutrients and pollutants in soils and associated environments. However, only a little of this vast research area has so far been investigated and understood. The novelty of the present study lies in the fact that it forms the first report of an original investigation disclosing the consequences of HyA- and HAS-interlayering/coating on Mt on the citrate-induced desorption kinetics of Se. It has also discovered the influences of silication of the complexing HyA ions on the desorption kinetics. The results of this study lead to three major conclusions: (1) HyA- and HAS-interlayering/coating on Mt increases the Se adsorption bond strength; (2) silication of the HyA ions prior to forming interlayers/coatings on Mt enhances the rates and reduced the E_a of Se desorption; and (3) the citrate ligand substantially enhances the desorption kinetics of pre-adsorbed Se from the clay surfaces, suggesting that citrate and possibly other low-molecular-weight organic ligands abundant in the rhizosphere play a significant role in mobilizing Se in soil environments. Thus, the findings of the present study are of considerable agro-environmental significance related to the dynamics of remobilization of Se in soil and associated environments.

ACKNOWLEDGMENTS

This study was supported by the Discovery Grant 2383-Huang of the Natural Sciences and Engineering Research Council of Canada.

REFERENCES

Aharoni, C. and Sparks, D.L. (1991) Kinetics of soil chemical reactions – a theoretical treatment. Pp. 1–18 in: *Rates of Soil Chemical Process* (D.L. Sparks and D.L. Suarez, editors). SSSA special publication, Soil Science Society of America, Madison, Wisconsin, USA.

Barnhisel, R.I. and P.M. Bertsch, P.M. (1989) Chlorites and hydroxy-interlayered vermiculite and smectite. Pp. 729–788 in: *Minerals in Soil Environments,* 2nd edition (J.B. Dixon and S.B. Weed, editors). SSSA Book Series no. 1, Soil Science Society of America, Madison, Wisconsin, USA.

Bautista-Tulin, A.T. and Inoue, K. (1997) Hydroxy-interlayered minerals in Japanese soils influenced by eolian deposition. *Soil Science Society of America Journal*, **61**, 631–640.

Benjamin, M.M. and Leckie, J.O. (1981) Multiple-site adsorption of Cd, Zn, and Pb on amorphous iron oxyhydroxide. *Journal of Colloid and Interface Science*, **79**, 209–221.

Bolan, N.S., Barrow, N.J. and Posner, A.M. (1985) Describing the effect of time on sorption of phosphate by iron and aluminum hydroxides. *Journal of Soil Science*, **36**, 187–197.

Bruckert, S. and Jacquin, F. (1969) Interaction entre la mobilite de plusieurs acides organiques et de diver cations dans un sol a mull et dans un sol a mor. *Soil Biology and Biochemistry*, **1**, 275–294.

Chien, S.H. and Clayton, W.R. (1980) Application of Elovich equation to the kinetics of phosphate release and sorption in soils. *Soil Science Society of America Journal*, **44**, 265–268.

Curl, E.A. and Truelove, B. (1986) *The Rhizosphere*. Springer-Verlag, Berlin.

Cushman, J.H. (1982) Nutrient transport inside and outside rhizosphere. Theory. *Soil Science Society of America Journal*, **46**, 704–709.

Dynes, J.J. and Huang, P.M. (1995) Influence of citrate on selenite sorption-desorption on short-range ordered aluminum hydroxides. Pp. 47–51 in: *Environmental Impact of Soil Component Interactions, Vol 2, Metals, Other Inorganics, and Microbial* Activities (P. M. Huang, J. Berthelin, J.-M. Bollag, W.B. McGill and A.L. Page, editors). CRC/Lewis Publishers, Boca Raton, Florida, USA.

Dynes, J.J. and Huang, P.M. (1997) Influence of organic acids on selenite sorption by poorly ordered aluminum hydroxides. *Soil Science Society of America Journal*, **61**, 772–783.

Eltantawy, I.M. and Arnold, P.M. (1973) Reappraisal of ethylene glycol mono-ethyl ether (EGME) method for surface area estimation of clays. *Journal of Soil Science*, **24**, 232–238.

Farmer, V.C., Fraser, A.R., Tait, J.M., Palmieri, F., Violante, P., Nakai, M. and Yoshinaga, N. (1978) Imogolite and proto-imogolite in an Italian soil developed on volcanic ash. *Clay Minerals*, **13**, 271–274.

Farmer, V.C., Fraser, A.R. and Tait, J.M. (1979) Characterization of chemical structures of natural and synthetic aluminosilicate gels and sols by infrared spectroscopy. *Geochimica et Cosmochimica Acta*, **43**, 1417–1420.

Harsh, J.B. and Doner, H.E. (1984) Specific adsorption of copper on a hydroxy-aluminum-montmorillonite complex. *Soil Science Society of America Journal*, **48**, 1034–1039.

Hayes, K.F., Roe, A.L., Brown Jr., G.E., Hodgson, K.O., Leckie, J.O. and Parks, G.A. (1987) In situ X-ray adsorption study of surface complexes: Selenium oxyanions on α-FeOOH. *Science (Washington, D.C.)*, **238**, 783–786.

Hingston, F.J. (1981) A review of anion adsorption. Pp. 51–90 in: *Adsorption of Inorganics in Solid-Liquid Interface* (M.A. Anderson and A.J. Rubin, editors). Ann Arbor Science, Ann Arbor, Michigan, USA.

Hingston, F.J., Posner, A.M. and Quirk, J.P. (1972) Anion adsorption by goethite and gibbsite. I. The role of the proton in determining adsorption envelopes. *Journal of Soil Science*, **23**, 177–189.

Hsu, P.H. (1968) Heterogeneity of the montmorillonite surface and its effect on the nature of hydroxy-aluminum interlayers. *Clays and Clay Minerals*, **16**, 303–311.

Huang, P.M. and Fujii, R. (1996) Selenium and arsenic. Pp. 793–831 in: *Methods of Soil Analysis. Part 3. Chemical Methods* (D.L. Sparks, editor). SSSA Book Series, No. *5*, Soil Science Society of America and American Agronomy Society of Agronomy, Madison, Wisconsin, USA.

Inoue, K. and Huang, P.M. (1984) Influence of citric acid on the natural formation of imogolite. *Nature (London)*, **308**, 58–60.

Inoue, K. and Satoh, C. (1992) Electric charge and surface characteristics of hydroxyaluminosilicate- and hydroxyaluminum-vermiculite complexes. *Clays and Clay Minerals*, **40**, 311–318.

Inoue, K. and Satoh, C. (1993) Surface charge characteristics of hydroxyaluminosilicate- and hydroxyaluminum-montmorillonite complexes. *Soil Science Society of America Journal*, **57,** 547–552.

Jackson, M.L (editor) (1979) *Soil Chemical Analysis – Advanced Course*, 2nd edition. Published by the author, Madison, Wisconsin, USA, 895 pp.

Krishnamurti, G.S.R., Huang, P.M. and Van Rees, K.C.J. (1997) Kinetics of cadmium release from soils as influenced by organic acids: Implication in cadmium availability.

Journal of Environment Quality, **26**, 271–277.
Lide, D.R. (2004) C*RC Handbook of Chemistry and Physics*, 85th edition. CRC Press, Boca Raton, Florida, USA.
Liu, C. and Huang, P.M. (2000) Kinetics of phosphate adsorption on iron oxides formed under the influence of citrate. *Canadian Journal of Soil Science*, **80**, 445–454.
Lothenbach, B., Furrer, G. and Schulin, R. (1997) Immobilization of heavy metals by polynuclear aluminum and montmorillonite compounds. *Environmental Science and Technology*, **31**, 1452–1562.
Lou, G. and Huang, P.M. (1988) Hydroxy-aluminosilicate interlayers in montmorillonite: implications for acidic environments. *Nature (London)*, **335**, 625–627.
Lou, G.Q.J. and Huang, P.M. (1994) Interlayer adsorption of hydroxy-aluminosilicate ions by montmorillonite. *Soil Science Society of America Journal*, **58**, 745–750.
Lou, G.Q.J. and Huang, P.M. (1995) Adsorption of hydroxyaluminosilicate ions by vermiculite. Pp. 187–191 in: *Clays Controlling the Environment* (G.J. Churchman, R.W. Fitzpatrick, and R.A. Eggleton, editors). *Proceedings of the 10th International Clay Conference*. CSIRO publishing, Melbourne, Australia.
Low, M.J.D. (1960) Kinetics of chemisorption of gases on solids. *Chemistry Review*, **6**, 267–312.
Madrid, L. and Arambarri, P. de. (1985) Adsorption of phosphate by two iron oxides in relation to their porosity. *Journal of Soil Science* **36**, 523–530.
Marel, H.W.V. and Beutelspacher, H. (1976) *Atlas of Infrared Spectroscopy of Clay Minerals and their Admixtures*. Elsevier Scientific Publishing Company, Amsterdam, The Netherlands, 396 pp.
Matsue, N. and Wada, K. (1988) Interlayer materials of partially interlayered vermiculite in Dystrochrepts derived from Tertiary sediments. *Journal of Soil Science*, **39**, 155–162.
Mehra, O.P. and Jackson, M.L. (1960) Iron oxide removal from soils and clays by a dithionite-citrate system buffered with sodium bicarbonate. Pp. 317–327 in: *7th Clays and Clay Minerals Proceedings of Conference*. Pergamon Press, London.
Neal, R.H. and Sposito, G. (1989) Selenate adsorption on alluvial soils. *Soil Science Society of America Journal*, **53**, 70–74.
Neal, R.H., Sposito, G., Holtzclaw, K.M. and Traina, S.J. (1987a) Selenite adsorption on alluvial soils: soil composition and pH effects. *Soil Science Society of America Journal*, **51**, 1161–1165.
Neal, R.H., Sposito, G., Holtzclaw, K.M. and Traina, S.J. (1987b) Selenite adsorption on alluvial soils: solution composition effects. *Soil Science Society of America Journal*, **51**, 1165–1169.
Nyquist, R.A. and Kagel, R.O. (1971) *Infrared Spectra of Inorganic Compounds*. Academic Press, San Diego, California, USA.
Parfitt, R.L., Fraser, A.R., Russell, J.D. and Farmer, V.C. (1977) Adsorption of hydrous oxides. II. Oxalate, benzoate, and phosphate on gibbsite. *Journal of Soil Science*, **28**, 40–47.
Pouchert, C.J. (1985) *The Aldrich Library of FT-IR Spectra*. Vol. 1&2, CRC Press, Boca Raton, Florida, USA.
Rovira, A.D. (1969) Plant root exudates. *Botanical Review*, **35**, 35–57.
Saeki, K. and Matsumoto, S. (1994) Selenite adsorption by a variety of oxides. *Communications in Soil Science and Plant Analyses*, **25**, 2147–2158.
Saha, U.K. and Inoue, K. (1997) Ammonium fixation by hydroxy-interlayered vermiculite and montmorillonite and its relation to potassium fixation. *Clay Science*, **10**, 133–150.
Saha, U.K., Hiradate, S. and Inoue, K. (1998) Retention of phosphate by hydroxyaluminum- and hydroxyaluminosilicate-montmorillonite complexes. *Soil Science Society of America Journal*, **62**, 922–929.
Saha, U.K., Taniguchi, S. and Sakurai, K. (2002) Simultaneous adsorption of cadmium, zinc, and lead on hydroxyaluminum- and hydroxyaluminosilicate-montmorillonite complexes. *Soil Science Society of America Journal*, **66**, 117–128.
Saha, U.K., Liu, C., Kozak, L.M. and Huang, P.M. (2004) Kinetics of selenite sorption on hydroxyaluminum- and hydroxyaluminosilicate-montmorillonite complexes. *Soil Science Society of America Journal*, **68**, 1197–1209.
Saha, U.K., Liu, C., Kozak, L.M. and Huang, P.M. (2005) Kinetics of selenite desorption by phosphate from hydroxyaluminum- and hydroxyaluminosilicate-montmorillonite complexes. *Geoderma*, **124**, 105–119.
Sakurai, K. and Huang, P.M. (1998) Intercalation of hydroxyaluminosilicate and hydroxyaluminum in montmorillonite and resultant physicochemical properties. *Soil Science Society of America Journal*, **62**, 362–368.
Sakurai, K., Ohdate, Y. and Kyuma, K. (1988) Comparison of salt titration and potentiometric titration methods for the determination of zero point of charge (ZPC). *Soil Science ant Plant Nutrition*, **34**, 171–182.
Scheidegger, A.M. and Sparks, D.L. (1996) A critical assessment of sorption-desorption mechanisms at the soil mineral/water interface. *Soil Science*, **161**, 814–831.
Schulthess, C.P. and Hu, Z. (2001) Impact of chloride anions on proton and selenium adsorption by aluminum oxide. *Soil Science Society of America Journal*, **65**, 710–718.
Sparks, D.L. (1989) *Kinetics of Soil Chemical Processes*. Academic Press, New York, USA.
Sparks, D.L. (1999) Kinetics of sorption/release reactions at the soil mineral/water interface. Pp. 135–191 in: *Soil Physical Chemistry*, 2nd edition (D.L. Sparks, editor). CRC Press, Boca Raton, Florida, USA.
Sparks, D.L. (2003) *Environmental Soil Chemistry*, 2nd edition. Academic Press, New York, USA. 352 pp.
Sparks, D.L. and Jardine, P.M. (1984) Comparison of kinetic equations to describe K-Ca in pure and mixed systems. *Soil Science*, **138**, 115–122.
Sterte, J. and Shabtai, J. (1987) Cross-linked smectites. V. Synthesis and properties of hydroxy-silicoaluminum montmorillonites and fluorhectorites. *Clays and Clay Minerals*, **3**, 429–439.
Stevenson, F.J. (1967) Organic acids in soil. Pp. 119–149 in: *Soil Biochemistry*. Vol. 1 (A.D. McLaren and G.H. Peterson, editors). Marcel Dekker, New York, USA.
Stevenson, F.J. (1991) Organic matter-micronutrient reactions in soil. Pp. 145–186 in: *Micronutrients in Agriculture*, 2nd edition (J.J. Mortvedt, F.R. Cox, L.M. Shuman and R.M. Welch, editors). Soil Science Society of America, Madison, Wisconsin, USA.
Stevenson, F.J. (1994) *Humus Chemistry. Genesis, Composition, Reactions*, 2nd edition. John Wiley & Sons, New York, USA.
Szmigielska, A.M., Van Rees, K.J.C., Cieslinski, G., Huang, P.M. and Knott, D.R. (1995) Determination of low molecular weight dicarboxylic acids in root exudates by gas chromatography. *Journal of Agriculture and Food Chemistry*, **43**, 956–959.
Szmigielska, A.M., Van Rees, K.J.C., Cieslinski, G., Huang, P.M. (1997) Comparison of liquid and gas chromatography for analysis of low-molecular-weight-organic acids in rhizosphere soil. *Communications in Soil Science and Plant Analyses*, **28**, 99–111.
Uren, N.C. and Raisenauer, H.M. (1988) The role of root exudates in nutrient acquisition. *Advances in Plant*

Nutrition, **3**, 79–114.
Wada, K. and Okamura, Y. (1980) Electric charge characteristics of Ando A1 and buried A1 horizon soils. *Journal of Soil Science*, **31**, 307–314.
Wada, S.-I. and Wada, K. (1980) Formation, composition and structure of hydroxyaluminosilicate ions. *Journal of Soil Science*, **31**, 457–467.
White, J.L. and Roth, C.B. (1986) Infrared spectroscopy. Pp. 291–330 in: *Methods of Soil Analysis Part 1*, 2nd edition (A. Klute, editor). Agronomy Monograph No. **9**, American Society of Agronomy and Soil Science Society of America, Madison, Wisconsin, USA.

(*Received 5 August 2005; revised 23 August 2006; Ms. 1084; A.E. James E. Amonette*)